

When are rough surfaces sticky?

Lars Pastewka^{1,2} and Mark O. Robbins¹

¹*Johns Hopkins University, Department of Physics and Astronomy,
3400 North Charles Street, Baltimore, MD 21218, USA*

²*Fraunhofer IWM, MikroTribologie Centrum μ TC,
Wöhlerstraße 11, 79108 Freiburg, Germany*

Abstract

At the molecular scale there are strong attractive interactions between surfaces, yet few macroscopic surfaces are sticky. Extensive simulations of contact by adhesive surfaces with roughness on nanometer to micrometer scales are used to determine how roughness reduces the area where atoms contact and thus weakens adhesion. The material properties, adhesive strength and roughness parameters are varied by orders of magnitude. In all cases the area of atomic contact rises linearly with load, and the prefactor rises linearly with adhesive strength for weak interactions. Above a threshold adhesive strength, the prefactor changes sign, the surfaces become sticky and a finite force is required to separate them. A parameter-free analytic theory is presented that describes changes in these numerical results over up to five orders of magnitude in load. It relates the threshold strength to roughness and material properties, explaining why most macroscopic surfaces do not stick. The numerical results are qualitatively and quantitatively inconsistent with classical theories based on the Greenwood-Williamson approach that neglect the range of adhesion and do not include asperity interactions.

Surfaces are adhesive or “sticky” if breaking contact requires a finite force. Few of the surfaces we encounter are sticky even though almost all are pulled together by van der Waals interactions at atomic scales.¹ Gecko setae^{2,3} and engineered adhesives⁴ use this ubiquitous attraction to achieve pull off forces per unit area that are orders of magnitude larger than atmospheric pressure, and our world would come to a halt if these pressures operated on most macroscopic surfaces.

The discrepancy between atomic and macroscopic forces has been dubbed the adhesion paradox.⁵ Experiments show that a key factor underlying this paradox is surface roughness, which reduces the fraction of surface atoms that are close enough to adhere.⁵⁻⁸ Quantitative calculations of this reduction are extremely challenging because of the complex topography of typical surfaces, which have bumps on top of bumps on a wide range of scales.^{9,10} In many cases they can be described as self-affine fractals from a lower wavelength λ_s of order nanometers to an upper wavelength λ_L in the micrometer to millimeter range.^{7,11} Here, we use an efficient Green’s function approach to calculate adhesive contact of surfaces with roughness from subnanometer to micrometer scales. Numerical results for a wide range of surfaces, adhesive interactions and material properties are presented and used to develop a simple, parameter-free equation that predicts the effect of adhesion on contact.

The traditional Greenwood-Williamson (GW)¹² approach for calculating contact of rough surfaces approximates their complex topography by a set of spherical asperities of radius R whose height distribution is determined from self-affine scaling. The long-range elastic interactions between different asperities are neglected. This approach is analytically tractable and provided a simple explanation for the observation that the area of contact between nonadhesive elastic surfaces is proportional to the normal force or load pushing them together. Later generalizations^{6,13} considered the effect of adhesion between surfaces and found that the key parameter was the ratio of the root mean squared (rms) height variation h_{rms} to the normal displacement δ_c of a single asperity due to adhesion. If the work of adhesion gained per unit area of contact is w , then $\delta_c^3 = (3/4)^3 R(\pi w/E^*)^2$ with contact modulus¹⁴ $E^* = E/(1 - \nu^2)$ for an isotropic material with Young’s modulus E and Poisson ratio ν . GW based adhesion models^{6,13} predict that the force needed to separate surfaces drops rapidly as h_{rms}/δ_c increases and is negligible for $h_{\text{rms}}/\delta_c > 3$.

In the last decade, Persson has developed a scaling theory that includes an approximate treatment of asperity interactions.^{15,16} At the same time, large scale numerical calculations of contact between rough surfaces have become feasible.¹⁷⁻²⁰ Both approaches reveal limitations in the GW treatment of nonadhesive surfaces. For example, the definition of R is ambiguous,²² the predicted

range of linear scaling between area and load is orders of magnitude too small,²³ and predictions for the geometry of individual contacts and the spatial correlations between them are qualitatively wrong.^{16,17} As shown below, these geometrical features determine the effect of adhesion.

In recent work, Persson has extended his theory to include adhesion in the limit where the range of surface separations over which attractive interactions are significant, Δr , is zero.^{15,24–26} He has applied this theory to specific cases and found a reduction in adhesion with increasing h_{rms} , but this powerful approach has not yet led to simple analytic predictions for general surfaces.

Here, we use an efficient Green’s function approach to calculate adhesive contact of surfaces with roughness from subnanometer to micrometer scales. The numerical results are clearly inconsistent with expressions based on the GW approximation. In particular, the relevant length scale describing the roughness is not h_{rms} and the range of adhesive interactions determines a characteristic adhesive pressure $w/\Delta r$ that plays a critical role. Numerical results for a wide range of surfaces, adhesive interactions and material properties are presented and used to develop a simple, parameter-free equation that predicts the effect of adhesion on contact.

RESULTS

Figure 1(a) shows the geometry of the simulations. There is a rigid upper surface with self-affine roughness. The change in height h over a lateral distance x increases as x^H where the Hurst exponent¹⁰ H is between 0 and 1. The elastic substrate is the (100) surface of an fcc crystal with atomic spacing a_0 , and behaves like a continuous medium in the limit of large λ_s/a_0 . We identify regions where atoms feel a repulsive force with the contact area A_{rep} (see methods).

Fig. 1(b) shows the complex spatial distribution of A_{rep} for nonadhesive interactions. Both GW and more recent approaches predict that A_{rep} is much smaller than the total area A_0 and rises linearly with the load N pushing the surfaces together.^{12,15,16,18–20} By dimensional analysis, the surface geometry can only enter through the dimensionless rms surface slope, $h'_{\text{rms}} = \sqrt{\langle |\nabla h|^2 \rangle}$ (see Fig. 1g). Steeper and stiffer surfaces are harder to bring into contact, so that^{12,15,16,18–21}

$$\frac{N}{A_{\text{rep}}} = \frac{h'_{\text{rms}} E^*}{\kappa_{\text{rep}}} \equiv p_{\text{rep}} , \quad (1)$$

where numerical solutions, such as the grey line in Fig. 2, find the dimensionless constant κ_{rep} is close to 2 while GW and Persson give $\kappa_{\text{rep}} \approx 2.6$ and 1.6, respectively. Note that the ratio of load to area represents the mean repulsive pressure p_{rep} in contacting regions, which depends only on h'_{rms} and E^* .

Figures 1(b)-(e) and 2 show how adding adhesion affects the distribution of contacting regions

and the relation between load and A_{rep} . There is no need to separately consider the effect of E^* and w because they always enter as a ratio with dimensions of length: $\ell_a \equiv w/E^*$. As discussed below, ℓ_a/a_0 is typically much less than unity and we use it to quantify the relative strength of adhesion.

Our first finding is that there is always a linear relation between the total load and the area in intimate repulsive contact at low N (Fig. 2). This can be described by Eq. (1) with κ_{rep} replaced by a renormalized constant κ . As the strength of adhesion increases, κ and the ratio of A_{rep} to load rise. Eventually the ratio diverges and the surfaces become sticky when κ changes sign. A negative κ leads to an elastic instability that pulls surfaces into contact and a pulloff force equal to the magnitude of the most negative load (see Fig. 2) is needed to separate them.

A quantitative model for the changes in κ can be derived by analyzing how adhesion affects contact geometry. Figures 1(c-e) show contacting regions (orange) that interact with repulsive forces and attracted regions (black) that are close enough to feel adhesive forces (Fig. 1(f,g)). The strength of adhesion is varied at constant total repulsive area A_{rep} . We find that the corresponding repulsive load N_{rep} and mean pressure p_{rep} also remain constant (see upper inset in Fig. 3) and that there are only minor morphological changes in the shape of A_{rep} . The main change is that the total area feeling an attractive force, A_{att} , spreads around the periphery of A_{rep} as the range of adhesive forces, Δr , increases (Fig. 1(e,f)). This type of behavior is assumed in the Derjaguin-Muller-Toporov (DMT) approximation for adhesion which is typically valid for spherical asperities in the nanometer and micrometer range.^{27,28} Different behavior might be observed if λ_s was much larger (Suppl. S-I).

The key observations needed to calculate κ are that p_{rep} remains constant, that there is a constant mean adhesive pressure $w/\Delta r$ in the attractive region (see Fig. 3) and that the ratio of repulsive and attractive areas is independent of load at low loads. The first two observations allow us to write the total load as $N = p_{\text{rep}}A_{\text{rep}} - (w/\Delta r)A_{\text{att}}$. From Eq. (1) we immediately find

$$1/\kappa = 1/\kappa_{\text{rep}} - 1/\kappa_{\text{att}} \quad (2)$$

with $\kappa_{\text{rep}} \approx 2$ and

$$\kappa_{\text{att}} = h'_{\text{rms}} \frac{\Delta r}{\ell_a} \frac{A_{\text{rep}}}{A_{\text{att}}} . \quad (3)$$

The remaining unknown is the ratio of repulsive to attractive area.

If $A_{\text{att}} \ll A_{\text{rep}}$, it can be approximated by $A_{\text{att}} \approx Pd_{\text{att}}$ where P is the length of the perimeter of A_{rep} and d_{att} the average lateral distance from the perimeter where the surface separation reaches

the interaction range Δr (Fig. 1(g)). For a general area, $A_{\text{rep}} = Pd_{\text{rep}}/\pi$ where d_{rep} is the mean diameter (see Fig. 1(f) and Suppl. S-II). For ordinary two dimensional objects like a circle, the perimeter and diameter are proportional and increase as the square root of the area. This behavior is assumed in conventional theories of contact between rough surfaces that ignore long-range elastic interactions between individual contacting asperities, such as the previously discussed GW¹² and related adhesive^{6,13,29} models. Including elastic interactions leads to qualitative changes in contact geometry.^{16–18} The contact area becomes a fractal with the same fractal dimension as the perimeter¹⁸ (a true “monster”¹⁰). We find that d_{rep} is then nearly independent of contact area, load and adhesive strength and present an analytic expression for it below.

We calculate d_{att} using continuum theory for nonadhesive contact of locally smooth surfaces. If x is the lateral distance from the edge of a contact, then for small x the separation between surfaces always¹⁴ rises as $x^{3/2}$. We use the standard prefactor for a cylinder with contact radius $d_{\text{rep}}/2$ and equate d_{att} to the lateral distance where the separation equals Δr (Suppl. S-I). Combined with our expression for P , this gives the constant ratio between attractive and repulsive areas

$$\frac{A_{\text{rep}}}{A_{\text{att}}} = \frac{d_{\text{rep}}}{\pi d_{\text{att}}} = \left[\frac{16}{9\pi} \right]^{1/3} \left[\frac{h'_{\text{rms}} d_{\text{rep}}}{\pi \Delta r} \right]^{2/3}. \quad (4)$$

Inserting this result in Eq. (3), gives the prediction for κ_{att} .

As shown in Fig. 4, our simple analytic expressions provide a quantitatively accurate description of $A_{\text{rep}}/A_{\text{att}}$ and $\kappa_{\text{rep}}/\kappa_{\text{att}}$ for a wide range of surface geometries. Deviations are only larger than the numerical uncertainty when the attractive area has grown too large to be approximated as a thin rim around the repulsive region (i.e. when $A_{\text{att}} > A_{\text{rep}}$), which is well into the sticky regime. The continuum expression for d_{att} also fails in this limit ($d_{\text{att}} > d_{\text{rep}}/2$).

Eqs. (3) and (4) provide a simple and quantitative explanation for the changes in Fig. 2. As the adhesion energy (and therefore ℓ_a) increases, there is a proportional increase in $1/\kappa_{\text{att}}$. At first adhesion merely produces a small change in the ratio of area to load. The sign of the ratio changes when $1/\kappa_{\text{att}}$ becomes bigger than $1/\kappa_{\text{rep}}$ and the surface becomes sticky.

The length d_{rep} is always of order λ_s and has a simple relation to statistical properties of the undeformed surface. As above and in Suppl. S-I, we approximate the contacting part of asperities by a cylinder with radius R , which is calculated from the rms curvature of the rough surface $1/R = h''_{\text{rms}}/2 = \sqrt{\langle (\nabla^2 h)^2 \rangle}/2$. If the contact has diameter d_{rep} and slope h'_{rms} at the contact edge, then $d_{\text{rep}} = 4h'_{\text{rms}}/h''_{\text{rms}}$. Following the same reasoning, the length in the numerator of Eq. (4) is

proportional to the height change δh from the contact edge to center:

$$\delta h = [h'_{\text{rms}}]^2 / h''_{\text{rms}} = h'_{\text{rms}} d_{\text{rep}} / 4 \quad (5)$$

The values of h'_{rms} and h''_{rms} can readily be evaluated from the statistical properties of the rough surface in real or reciprocal space. The lower inset of Fig. 3 shows that P and A_{rep} are proportional and that the proportionality constant is always within a factor of two of $4h'_{\text{rms}}/h''_{\text{rms}}$.

The contact area is not directly accessible to experiment, but changes with load in the mean separation between surfaces u can be measured with sufficiently stiff mechanical devices.^{30,31} The normal contact stiffness defined as $k_N = dN/du$ is typically found to rise linearly with load for nonadhesive surfaces.^{32,33} In the regime where surfaces are not sticky we find that the relation between surface separation and N_{rep} is nearly unchanged, just as the relation between N_{rep} and A_{rep} is nearly the same (Fig. 3 upper inset). Since adhesion reduces the total load N by a factor of $\kappa_{\text{rep}}/\kappa$, the normal stiffness is reduced by the same factor. This is a small correction unless the surfaces are close to becoming sticky, and nonadhesive predictions are likely to be within experimental uncertainties.

DISCUSSION

Surfaces are sticky when the total adhesive force, which is adhesive pressure times attractive area, exceeds the total repulsive force $p_{\text{rep}}A_{\text{rep}}$. This corresponds to $1/\kappa_{\text{att}} > 1/\kappa_{\text{rep}}$, and our numerical results show stickiness if and only if this condition is met. It can be recast as a condition on the ratios of pressures and areas, $(w/\Delta r)/p_{\text{rep}} > A_{\text{rep}}/A_{\text{att}}$, or using our analytic expressions:

$$\frac{h'_{\text{rms}}\Delta r}{\kappa_{\text{rep}}\ell_a} \left[\frac{\delta h}{\Delta r} \right]^{2/3} < \pi \left[\frac{3}{16} \right]^{2/3} \approx 1 \quad (6)$$

where the first factor on the left reflects the pressure ratio and the second comes from the area ratio. As noted above and in the supplementary material the effective range of the potential is typically less than but of order of the atomic bond-distance a_0 . Any height change δh is possible in continuum theory, but there is a natural lower bound of order a_0 in atomic systems. For example, roughness on crystalline surfaces occurs in the form of terraces with height $\sim a_0$. Inserting this bound in Eq. (4) one finds a necessary but not sufficient criterion for adhesion: $\ell_a/a_0 \gtrsim 0.5h'_{\text{rms}}$.

Note that the above prediction for the onset of adhesion is qualitatively different than previous models for rough surface adhesion, which do not include two of the key lengths in Eqs. (3)–(6). The characteristic width of contacting regions d_{rep} reflects their fractal nature and has not been identified before. Continuum theories have considered the limiting cases of Δr equal to zero^{6,15,29}

or infinity¹³ and concluded Δr had little effect,¹³ while we find more adhesion at small Δr because the adhesive pressure is increased. Finally, our relations only include quantities that are determined by short wavelength roughness – the rms surface slope and curvature. The rms roughness is the key surface property in past GW theories, and rises with the upper wavelength of roughness as λ_L^H . The numerical results with different symbol size in Fig. 4 have values of λ_L^H that vary by more than an order of magnitude but collapse onto the universal curve predicted by Eqs. (3) and (4). Supplemental section S-III presents plots that show qualitative discrepancies between these data and traditional GW theories.

To determine the implications of Eq. (6), we first consider the extreme case where w is the adhesive energy for joining crystals of the same material. Then for atomistic solids the same interactions determine both E^* and w . The value of ℓ_a is of order of the relative displacement needed to change the elastic energy by the binding energy, and $\ell_a/a_0 \ll 1$. For example, diamond has $E^* \approx 10^{12}$ Pa and $w \approx 10$ J/m², yielding $\ell_a/a_0 \approx 0.06$ with a_0 the carbon bond length. The simple Lennard-Jones potential has $\ell_a/a_0 \approx 0.05$. For these typical values of ℓ_a , adhesion should occur for h'_{rms} of order 0.1 and below. The stickiest cases considered in Fig. 4 (closed red symbols) are indeed for the case $\ell_a/a_0 = 0.05$, $h'_{\text{rms}} = 0.1$, and small d_{rep} . Increasing h'_{rms} to 0.3 suppresses adhesion.

Exposing surfaces to the environment typically reduces the adhesive forces to van der Waals interactions with $w \sim 50$ mJ/m². The value of ℓ_a and the root mean square slope needed to eliminate adhesion are reduced by two to three orders of magnitude. Only exceptionally smooth surfaces like atomically flat mica¹ and the silicon surfaces used in wafer bonding³⁴ have slopes low enough to stick ($\lesssim 10^{-3}$). For most surfaces $\kappa \approx \kappa_{\text{rep}}$. This provides an explanation for the success of models for friction that ignore van der Waals adhesion.^{12,14,28,35}

Most of the sticky surfaces we are familiar with break the connection between w and E^* to increase ℓ_a/a_0 . Geckos^{2,3} and recently manufactured mimics⁴ break the solid up into a hierarchical series of separate rods with pads at the ends. This allows adjacent pads to contact the surface at different heights without a large elastic energy, leading to a small effective E^* even though the components are stiff. Tape, rubber, and elastomers adhere via van der Waals interactions, but have small elastic moduli associated with the entropy required to stretch polymer segments between chemical crosslinks. Eq. (6) implies that surfaces with $w = 50$ mJ/m², $h'_{\text{rms}} \sim 1$, $\Delta r \sim 0.5$ nm and $d_{\text{rep}} \sim 10$ nm will be sticky if $E^* \lesssim 10$ MPa, which is common for soft rubbers and elastomers while paper is much stiffer (>1 GPa). Tapes are normally designed to have moduli below 0.1MPa,

which is known as the Dahlquist criterion.³⁶ Taking $h'_{\text{rms}} \sim 1$ and $\Delta r \sim 0.5$ nm, one finds adhesion for $d_{\text{rep}} \lesssim 100$ μm . Adhesives of this type can stick even to structured surfaces with macroscopic grooves. Once an adhesive bond is formed, the viscoelastic properties of the adhesive that can be used to greatly increase the force needed to break the adhesive bond.⁵

In summary, we have presented numerical simulations of adhesive contact between rough surfaces for a wide range of adhesion strength, surface geometries and material properties. In all cases the area in intimate repulsive contact rises linearly with the applied load at low loads. The ratio of area to load increases with adhesion and changes sign when surfaces begin to stick. This transition only occurs in the limits of smooth surfaces, high surface energy and low stiffness. The results are qualitatively inconsistent with traditional GW theories, but in quantitative agreement with a simple parameter-free theory based on observed changes in contact geometry. This theory makes specific predictions for experimental systems and may aid in the design of adhesives, and in engineering surface roughness to enhance or eliminate adhesion. It also provides a simple explanation for our everyday experience with macroscopic adhesion. For most materials the internal cohesive interactions that determine elastic stiffness are stronger than adhesive interactions and surfaces will only stick when they are extremely smooth. Tape, geckos and other adhesives stick because the effect of internal bonds is diminished to make them anomalously compliant.

Methods — Calculations were performed for a rigid rough surface contacting a flat elastic substrate. In continuum theory this is equivalent to contact between two rough elastic surfaces and the mapping remains approximately valid at atomic scales.³⁷ Self-affine rough surfaces with the desired Hurst exponent H , h'_{rms} , λ_s and λ_L are generated using a Fourier-filtering algorithm described previously.³⁸ Fourier components for each wavevector \vec{q} have a random phase and a normally distributed amplitude that depends on the magnitude q . The amplitude is zero for $q > 2\pi/\lambda_s$, proportional to q^{-1-H} for $2\pi/\lambda_s > q > 2\pi/\lambda_L$, and rolls over to a constant for $q < 2\pi/\lambda_L$. Periodic boundary conditions with period L are applied in the plane of the surface to prevent edge effects. The elastic response is determined using a Fourier-transform technique^{39,40} with a linearised surface Green's function corresponding to Poisson ratio $\nu = 1/2$. Results are shown for period $L = 2\lambda_L = 4096a_0$ with rigid boundary conditions applied at depth L below the surface. Systematic studies were performed with L and λ_L from $512a_0$ to $8192a_0$ to ensure that finite-size effects are small.

Atoms on the elastic substrate interact with the rigid rough surface through a potential that only depends on the height difference z . We use a 9-3 Lennard-Jones potential that represents the integral over a half space of the usual 12-6 Lennard-Jones potential between atoms. The potential is truncated smoothly using a cubic spline from the potential minimum at $z = a_0$ to the cutoff at $a_0 + \Delta r$. The potential and its first two derivatives are continuous and vanish at the cutoff. In our calculations we fix the stiffness k of the potential at a value that is consistent with the stiffness of interactions within the substrate: $k = E^*a_0/2$. Consistent results were obtained with other potentials, including an untruncated 12-6 Lennard-Jones potential.

As is common for atomic-scale calculations,^{37,41,42} the contact area A_{rep} is defined as the area covered by atoms that feel a repulsive force ($z < a_0$). Similarly, the attractive area A_{att} is the area covered by atoms that feel an attractive force ($a_0 < z < a_0 + \Delta r$). We only show results for $A_{\text{rep}}/\lambda_s^2 \gtrsim 10$, so that there is a statistical number of contacting asperities.¹⁸ Numerical values of κ , κ_{rep} and κ_{att} are computed at 1% contact area from the ratios of load and area.

Acknowledgements — This work was supported by the Air Force Office of Scientific Research (grant FA9550-0910232), the U.S. National Science Foundation (grant OCI-108849, DMR-1006805, CMMI-0923018), the Simons Foundation (M.O.R.) and the European Commission (Marie-Curie IOF 272619 for L.P.). Computations were carried out at Johns Hopkins University and the Jülich Supercomputing Center.

-
- ¹ Israelachvili JN (2011) *Intermolecular and Surface Forces* (Academic Press, London), 3rd ed.
 - ² Autumn K *et al.* (2000) Adhesive force of a single gecko foot-hair. *Nature* 405:681-685.
 - ³ Autumn K *et al.* (2002) Evidence for van der Waals adhesion in gecko setae. *Proc Natl Acad Sci USA* 99:12252-12256.
 - ⁴ Geim AK *et al.* (2003) Microfabricated adhesive mimicking gecko foot-hair. *Nature Mater* 2:461-463.
 - ⁵ Kendall K (2001) *Molecular Adhesion and Its Applications: The Sticky Universe* (Kluwer Academic/Plenum Publishers, New York).
 - ⁶ Fuller KNG, Tabor D (1975) The effect of surface roughness on the adhesion of elastic solids. *Proc R Soc Lond A* 345:327-342.
 - ⁷ Persson BNJ, Albohr O, Tartaglino U, Volokitin AI, Tosatti E (2005) On the nature of surface roughness with application to contact mechanics, sealing, rubber friction and adhesion. *J Phys Condens Matter* 17:R1-R62.
 - ⁸ Jacobs TDB *et al.* (2013) The effect of atomic-scale roughness on the adhesion of nanoscale asperities: A combined simulation and experimental investigation. *Tribol Lett* 50:81-93.
 - ⁹ Whitehouse DJ, Archard JF (1970) The properties of random surfaces of significance in their contact. *Proc R Soc Lond A* 316:97-121.
 - ¹⁰ Mandelbrot BB (1982) *The Fractal Geometry of Nature* (W. H. Freeman).
 - ¹¹ Mandelbrot BB, Passoja DE, Paullay AJ (1984) Fractal character of fracture surfaces of metals. *Nature* 308:721-722.
 - ¹² Greenwood JA, Williamson JBP (1966) Contact of nominally flat surfaces. *Proc R Soc Lond A* 295:300-319.
 - ¹³ Maugis D (1996) On the contact and adhesion of rough surfaces. *J Adhesion Sci Technol* 10:161-175.
 - ¹⁴ Johnson KL (1985) *Contact Mechanics* (Cambridge University Press).
 - ¹⁵ Persson BNJ (2002) Adhesion between elastic bodies with randomly rough surfaces. *Phys Rev Lett* 89:245502.
 - ¹⁶ Persson BNJ (2008) On the elastic energy and stress correlation in the contact between elastic solids with randomly rough surfaces. *J. Phys.: Condens. Matter* 20:312001.
 - ¹⁷ Campañá C, Müser MH, Robbins MO (2008) Elastic contact between self-affine surfaces: comparison of numerical stress and contact correlation functions with analytic predictions. *J Phys Condens Matter*

20:354013.

- 18 Hyun S, Pei L, Molinari J-F, Robbins MO (2004) Finite-element analysis of contact between elastic self-affine surfaces. *Phys. Rev. E* 70:026117.
- 19 Campañá C, Müser MH (2007) Contact mechanics of real vs. randomly rough surfaces: A Green's function molecular dynamics study. *Europhys. Lett.* 77:38005.
- 20 Putignano C, Afferrante L, Carbone G, Demelio G (2012) The influence of the statistical properties of self-affine surfaces in elastic contacts: A numerical investigation. *J Mech Phys Solids* 60:973-982.
- 21 Yastrebov V, Anciaux G, Molinari J-F (2012) Contact between representative rough surfaces. *Phys Rev E* 86:035601.
- 22 Greenwood J, Wu J (2001) Surface roughness and contact: An apology. *Meccanica* 36:617-630.
- 23 Carbone G, Bottiglione F (2008) Asperity contact theories: Do they predict linearity between contact area and load?. *J Mech Phys Solids* 56:2555-2572.
- 24 Persson BNJ, Tosatti E (2001) The effect of surface roughness on the adhesion of elastic solids. *J Chem Phys* 115:5597-5610.
- 25 Peressadko A, Hosoda N, Persson BNJ (2005) Influence of surface roughness on adhesion between elastic bodies. *Phys Rev Lett* 95:124301.
- 26 Mulakaluri N, Persson BNJ (2011) Adhesion between elastic solids with randomly rough surfaces: Comparison of analytical theory with molecular-dynamics simulations. *EPL* 96:66003.
- 27 Maugis D (1992) Adhesion of spheres: The JKR-DMT transition using a Dugdale model. *J Colloid Interf Sci* 150:243-269.
- 28 Carpick RW, Ogletree DF, Salmeron M (1999) A general equation for fitting contact area and friction vs load measurements. *J Colloid Interf Sci* 211:395-400.
- 29 Chow TS (2001) Nanoadhesion between rough surfaces. *Phys Rev Lett* 86:4592-4595.
- 30 Oliver WC, Pharr GM (1992) An improved technique for determining hardness and elastic modulus using load and displacement sensing indentation experiments. *J Mater Sci* 7: 1564-1583.
- 31 Carpick RW, Ogletree DF, Salmeron M (1997) Lateral stiffness: A new nanomechanical measurement for the determination of shear strengths with friction force microscopy. *Appl Phys Lett* 70:1548-1550.
- 32 Akarapu S, Sharp T, Robbins MO (2011) Stiffness of contacts between rough surfaces. *Phys Rev Lett* 106:204301.
- 33 Campañá C, Persson BNJ, Müser MH (2011) Transverse and normal interfacial stiffness of solids with randomly rough surfaces. *J Phys Condens Matter* 23:085001.

- ³⁴ Tong QY, Gösele UM (1999) Wafer bonding and layer splitting for microsystems. *Adv Mater* 11:1409-1425.
- ³⁵ Bowden FP, Tabor D, (1950) *The Friction and Lubrication of Solids* (Oxford University Press).
- ³⁶ Creton C, Leibler L (1996) How does tack depend on time of contact and contact pressure? *J Polym Sci Pol Phys* 34:545-554.
- ³⁷ Luan B, Robbins MO (2005) The breakdown of continuum models for mechanical contacts. *Nature* 435:929-932.
- ³⁸ Ramisetti SB *et al.* (2011) The autocorrelation function for island areas on self-affine surfaces. *J Phys Condens Matter* 23:215004.
- ³⁹ Pastewka L, Sharp TA, Robbins MO (2012) Seamless elastic boundaries for atomistic calculations. *Phys Rev B* 86:075459.
- ⁴⁰ Campañá C, Müser MH (2006) Practical Green's function approach to the simulation of elastic semi-infinite solids. *Phys Rev B* 74:075420.
- ⁴¹ Mo Y, Turner KT, Szlufarska I (2009) Friction laws at the nanoscale. *Nature* 457:1116-1119.
- ⁴² Knippenberg, MT, Mikulski, PT, Dunlap, BI, Harrison, JA (2008) Atomic contributions to friction and load for tip–self-assembled monolayers interactions. *Phys Rev B* 78:235409.

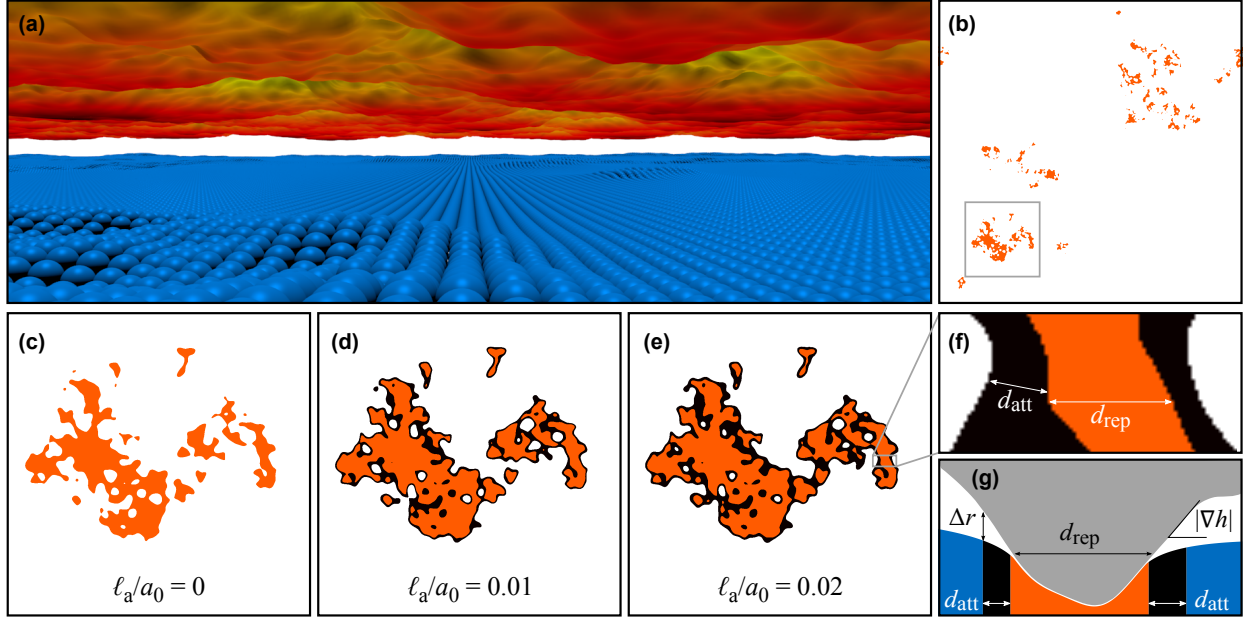


FIG. 1: **Contact geometry.** (a) The rigid top surface is a self-affine fractal with Hurst exponent $H = 0.8$, root mean square slope $h'_{\text{rms}} = 0.1$, lower wavelength cutoff $\lambda_s = 32a_0$ and upper wavelength cutoff $\lambda_L = 2048a_0$. The elastic substrate is initially flat with atoms spaced by a_0 . Substrate deformations produced by a typical adhesive contact are shown. All height variations are magnified to show on the scale of the figure. (b-e) Atoms that feel repulsive (orange) and attractive (black) forces at a fixed $A_{\text{rep}} \sim 0.02A_0$. Nonadhesive results for the entire system are shown in (b) and expanded views of the region indicated by a square are shown in (c-e) for the indicated $w/E^*a_0 = \ell_a/a_0$. (f) Magnified view of an $80a_0$ wide region of (e). The mean diameter d_{rep} is obtained by averaging the distance across A_{rep} . (g) Vertical slice through a contact patch showing the rigid rough (gray) surface and the deformed elastic substrate. The root mean square slope, h'_{rms} , is the rms average of the local slope, $|\nabla h|$, as indicated on the right. The attractive length d_{att} is the distance from the repulsive patch edge at which the gap equals the interaction range Δr . The surface separation rises as a $3/2$ power law for nonadhesive surfaces, leading to the $2/3$ exponent in Eq. (4).

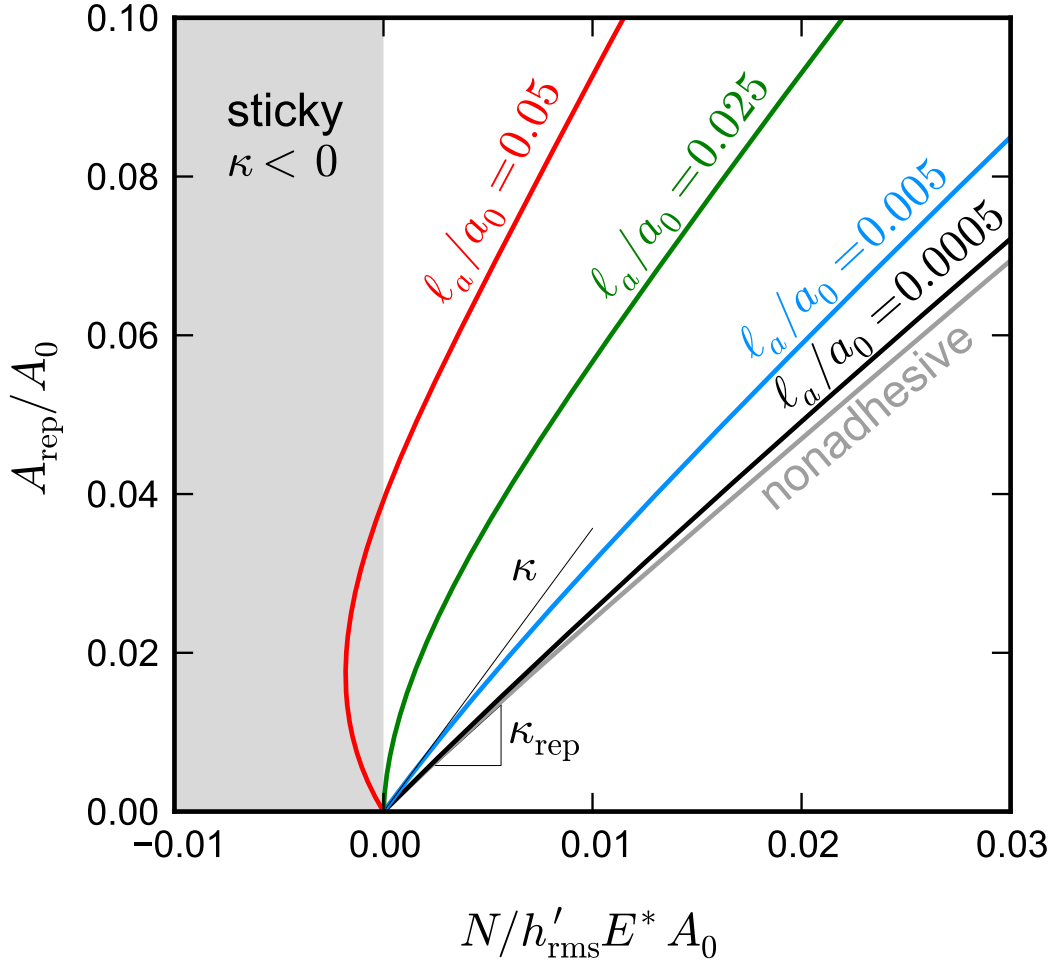


FIG. 2: **Contact area as a function of normal load.** For nonadhesive contact, the contact area A_{rep} rises approximately linearly with load N with dimensionless prefactor $\kappa_{\text{rep}} \approx 2$ (Eq. 1). As the strength of adhesion $\ell_a = w/E^*$ increases, the area rises more rapidly with load. The initial ratio of area to load corresponds to a renormalized κ that diverges at the onset of stickiness (green line). The red line shows a sticky case where $\kappa < 0$ and the pull-off force is nonzero. Results shown are for a surface with Hurst exponent $H = 0.8$, root mean square slope $h'_{\text{rms}} = 0.1$, and lower wavelength cutoff $\lambda_s = 32a_0$.

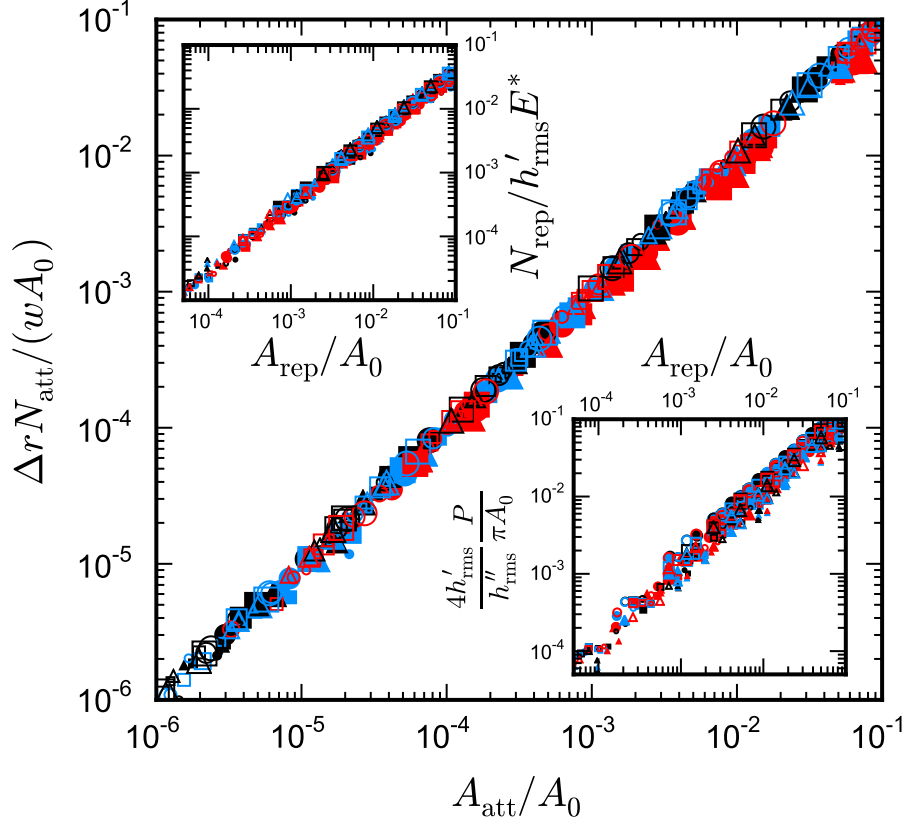


FIG. 3: **Test of predictions for N_{rep} and N_{att} .** The attractive load N_{att} is equal to the attractive area A_{att} times the mean adhesive pressure $w/\Delta r$. Upper inset: The repulsive load N_{rep} is equal to the repulsive area A_{rep} times the mean repulsive pressure $p_{\text{rep}} \equiv h'_{\text{rms}} E^*/\kappa_{\text{rep}}$ where κ_{rep} remains close to 2 even for the adhesive case with finite ℓ_a . Lower inset: The length of the perimeter P of the repulsive area A_{rep} is proportional to the area itself. Plot is normalized to show that $d_{\text{rep}} \equiv \pi A_{\text{rep}}/P$ is nearly independent of A_{rep} and $d_{\text{rep}} \approx 4h'_{\text{rms}}/h''_{\text{rms}}$. Deviations by up to a factor of 2 from this expression for d_{rep} are responsible for the spread in the figure. For a given system, changes in d_{rep} with A_{rep} are less than 25% over 2-3 decades in A_{rep} . All plots show multiple contact areas for each realization of a surface. Results are shown for $H = 0.3$ (triangles), 0.5 (squares) and 0.8 (circles) and $\ell_a/a_0 = 0.0005$ (black), 0.005 (blue) and 0.05 (red). Closed and open symbols are for $h'_{\text{rms}} = 0.1$ and 0.3, respectively. The symbol size increases as λ_s/a_0 increases from 4 to 64 in powers of 2.

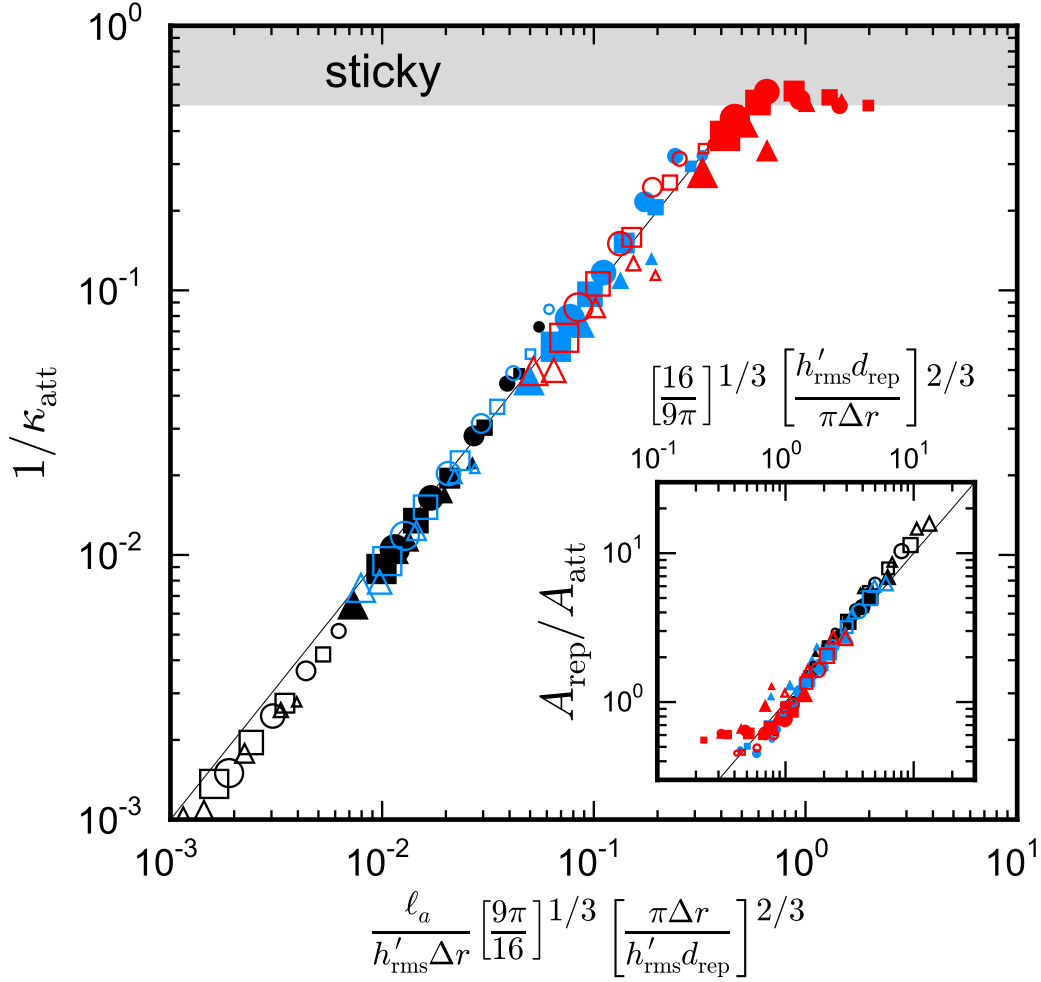


FIG. 4: **Test of predictions for κ_{att} and A_{att} .** The attractive $1/\kappa_{\text{att}}$ is plotted against the prediction in Eq. (3). The solid line has unit slope. Results are shown for Hurst exponents $H = 0.3$ (triangles), 0.5 (squares) and 0.8 (circles) and adhesive strengths $\ell_a/a_0 = 0.0005$ (black), 0.005 (blue) and 0.05 (red). Closed and open symbols are for root mean square slopes $h'_{\text{rms}} = 0.1$ and 0.3 , respectively. The symbol size increases as the lower wavelength cutoff λ_s/a_0 increases from 4 to 64 in powers of 2. Adhesion is observed if and only if $1/\kappa_{\text{att}} > 1/\kappa_{\text{rep}}$. The shaded region shows the prediction for adhesion using the value $\kappa_{\text{rep}} = 2$ found in the continuum limit (Suppl. S-2). Inset: Plot of the ratio of repulsive to attractive area $A_{\text{rep}}/A_{\text{att}}$ against the prediction of Eq. (4).

Supplementary Material for “When are rough surfaces sticky?”

Lars Pastewka^{1,2} and Mark O. Robbins¹

¹ Johns Hopkins University, Dept. Physics and Astronomy, Baltimore, MD 21218, USA

² Fraunhofer IWM, MikroTribologie Centrum μ TC, 79108 Freiburg, Germany

S-I. SURFACE SEPARATION, d_{att} , AND THE EFFECTIVE RANGE Δr FOR ARBITRARY INTERACTION POTENTIALS

As discussed in the main text, we use standard results from continuum theory for nonadhesive contact between smooth surfaces. If x is the lateral distance from the edge of the contact, then for small x the separation $\Delta(x)$ between surfaces always rises as $x^{3/2}$ outside the contact.¹ The prefactor rises with the surface slope at the edge of the contact which we take to be h'_{rms} . For simple geometries like spheres, cones or cylinders, the only length scale that enters is the radius of the contact area. Since the contacting region in our numerical simulations has a constant average diameter d_{rep} , we use the standard prefactor for a cylinder:^{2,3}

$$2 \frac{\Delta(x)}{d_{\text{rep}}} = \frac{\sqrt{8}}{3} h'_{\text{rms}} \left(\frac{2x}{d_{\text{rep}}} \right)^{3/2} \quad (\text{S-1})$$

Our numerical data for the average surface separation at a given distance from the perimeter are consistent with this relation without adjustable parameters. To find d_{att} we just equate $\Delta(d_{\text{att}})$ to Δr in Eq. (S-1), yielding

$$d_{\text{att}}/d_{\text{rep}} = \left(\frac{3}{4} \frac{\Delta r}{h'_{\text{rms}} d_{\text{rep}}} \right)^{2/3}. \quad (\text{S-2})$$

An effective range of interaction Δr can be defined for arbitrary forms of the interaction potential using Eq. (S-1). We define $p(\Delta)$ as the attractive pressure between surfaces separated by $\Delta > 0$. Then $w = \int_0^{\infty} d\Delta p(\Delta)$ where w is the work of adhesion. As in the calculation of A_{att} in the main document, we assume that the perimeter changes direction slowly enough that we can write the total load as the perimeter times a contribution per unit length. With $\Delta(x)$ being the separation

at distance x from the contact edge, this yields:

$$N_{\text{att}} = P \int_0^{\infty} dx p(\Delta(x)) . \quad (\text{S-3})$$

This is equivalent to the expressions in the main text for truncated potentials with

$$d_{\text{att}}/\Delta r = \int_0^{\infty} dx p(\Delta(x))/w . \quad (\text{S-4})$$

From Eqs. (S-1), (S-2) and (S-4) one finds an expression for Δr

$$(\Delta r)^{-1/3} = \frac{2}{3} \int_0^{\infty} d\Delta \Delta^{-1/3} p(\Delta) \Big/ \int_0^{\infty} d\Delta p(\Delta) . \quad (\text{S-5})$$

With this value of Δr , all of the relations in the main text for truncated potentials carry over to an arbitrary potential. Note that the integrals are well defined because p represents the total force and goes linearly to zero at the equilibrium surface separation $\Delta = 0$.

In general we find that Δr from Eq. (S-5) is comparable to or smaller than the atomic spacing a_0 that minimizes the energy. For example, if the 9-3 Lennard-Jones potential is used to infinite distances, one finds $\Delta r = 1.15a_0$. For the 12-6 Lennard-Jones potential, $\Delta r = 0.62a_0$. Note that these ranges are referenced to the potential minimum at a_0 and that most of the binding energy comes from these short scales ($> 85\%$).

The spline potential used in the calculations reported in the main text has

$$p(z) = \frac{k}{a_0^2} \begin{cases} \frac{a_0}{6} \left[\left(\frac{a_0}{z}\right)^{10} - \left(\frac{a_0}{z}\right)^4 \right] & \text{if } z \leq a_0 \\ -(z - a_0) + \frac{2}{\Delta r}(z - a_0)^2 - \frac{1}{\Delta r^2}(z - a_0)^3 & \text{if } a_0 < z < a_0 + \Delta r \\ 0 & \text{if } z > a_0 + \Delta r \end{cases} \quad (\text{S-6})$$

where a_0 is the minimum of the potential and $k = E^* a_0/2$ is the stiffness at $z = a_0$. The adhesion energy was varied by changing Δr at fixed k . The range given by Eq. (S-5) for this potential is essentially the same as the actual range (within 6%). For a general truncated potential, quantitative agreement with results for the relation between area and load are better when Eq. (S-5) is used.

In calculating the load we have assumed that the variation of the surface separation Δ with x is not affected by adhesion. A similar approximation is made in the Derjaguin-Muller-Topov (DMT) theory for contact of a spherical asperity of radius R .⁴ Maugis has found that the DMT approximation is accurate for spheres when a dimensionless ratio λ_{Maugis} is small:⁵

$$\lambda_{\text{Maugis}} \equiv \left[\frac{9R\ell_a^2}{2\pi(\Delta r)^3} \right]^{1/3} . \quad (\text{S-7})$$

As above and in the main text, we determine $R = d_{\text{rep}}/2h'_{\text{rms}}$ by assuming a locally cylindrical geometry with contact diameter d_{rep} and slope h'_{rms} at the edge of the contact. We find that the approximations used in the main text are accurate even when λ_{Maugis} exceeds unity. Using typical values of $\ell_a \sim 5 \cdot 10^{-4}$ for atomistic solids exposed to the environment, $h'_{\text{rms}} = 0.1$ and $\Delta r/a_0 = 1$, this corresponds to d_{rep} of close to a millimeter. For elastomers and other compliant systems, surface deformation becomes important at smaller scales, but the surfaces are usually sticky and other corrections are also required. For example, A_{att} is typically not small compared to A_{rep} . Previous analytic studies of rough surface adhesion have considered the Johnson-Kendall-Roberts (JKR) limit where the area outside the contact does not contribute significantly to the adhesion.⁶ This corresponds to $\lambda_{\text{Maugis}} > 5$ where the contact radius becomes of macroscopic dimensions.

Finally, many of the above relations assume that the surface slope is relatively small so that the total and projected areas are nearly equal and the potential interaction depends only on the vertical separation. The strains induced by contact are of order the surface slope and plasticity also becomes important for very steep surfaces.

S-II. DETERMINING CONTACT PATCH GEOMETRIES

For continuous curves, the perimeter and area are related through d_{rep} , the mean length of contiguous segments in horizontal (or vertical) slices through A_{rep} (see Fig. 1(f) in main text). Suppose the slices are made at a spacing dz that can be made arbitrarily small. The total area can be approximated by the sum over all contiguous segments of the segment length times dz . If the total number of segments is N_{tot} , then $A_{\text{rep}} = N_{\text{tot}}d_{\text{rep}}dz$. Each end of a segment contributes dz to the projection of the perimeter perpendicular to the slice. The projected perimeter length is then $2N_{\text{tot}}dz$. The total perimeter length is $\pi N_{\text{tot}}dz$ if one assumes that all orientations are sampled equally – as for a circle. This gives the relation $A_{\text{rep}} = Pd_{\text{rep}}/\pi$ cited in the text.

Figure S-1 illustrates how area and perimeter are defined on the discrete geometry used in our simulations. Atoms on the substrate surface form a square grid with spacing a_0 . The surface is divided into a grid of square cells centered on each atom. A grid cell contributes a_0^2 to A_{rep} if the corresponding atom feels a repulsive force and to A_{att} if the force is attractive.

Grid cells are defined to be neighbors if they share an edge (Fig. S-1a). The corresponding atoms are then nearest neighbors. The repulsive area is divided into connected patches like that shown in Fig. S-1b. Grid cells (atoms) that belong to a patch but have less than four neighbors in

the patch are part of the perimeter. The perimeter length P is calculated as: $P = \beta a_0 N_P$ where N_P is the number of perimeter cells and β corrects for the discreteness of the lattice. Consider a line of length L at an angle θ to the horizontal axis. The perimeter cells will form a stepped approximation to this line. It is easy to show that the number of perimeter cells is equal to $L/(a_0 \cos \theta)$ for θ between $-\pi/4$ and $\pi/4$. Counting these cells and multiplying by a_0 underestimates P by a factor of $1/\cos \theta$. We find $\beta = 4 \sinh^{-1}(1)/\pi \approx 1.1222$ by assuming isotropy and averaging over angles.

Figure S-2 tests the above relations by plotting the predicted ratio of perimeter to area as a function of d_{rep} for the full range of H , λ_s and w discussed in the main text. Agreement is excellent in the continuum limit. For $d_{\text{rep}}/a_0 > 10$ results are within the numerical uncertainty. The deviation at the greatest d_{rep} is reduced if λ_L/d_{rep} is increased to remove finite-size effects. As d_{rep}/a_0 decreases below 10, there is an accelerating drop in the plotted ratio. The above relations assumed lines were straight, and curvature can not be ignored when the radius of curvature of the perimeter, $\sim d_{\text{rep}}/2$, is comparable to the grid spacing, a_0 .

S-III. COMPARISON TO THEORIES BASED ON THE GREENWOOD-WILLIAMSON APPROXIMATION

As noted in the main text, traditional theories for the effect of adhesion start from the Greenwood-Williamson approximation. Fuller and Tabor⁷ found the pulloff force needed to separate the surfaces in the JKR limit of short range potentials ($\Delta r \rightarrow 0$) and Maugis⁸ found similar results for the opposite DMT limit of long range potentials ($\Delta r \rightarrow \infty$). In both cases, the pulloff force is a function of h_{rms}/δ_c , where δ_c is the normal displacement of a single asperity due to adhesion $\delta_c^3 = (3/4)^3 R(\pi w/E^*)^2$. The pulloff force drops rapidly for $h_{\text{rms}}/\delta_c > 1$ and is extremely small for $h_{\text{rms}}/\delta_c > 3$. In contrast to our results, no clear transition to nonadhesive behavior with area proportional to load was discussed.

These traditional theories expressed the pulloff force as a ratio to the maximum force NP_c where N is the number of spherical asperities and $P_c = 3\pi wR/2$ the pulloff force for each in the JKR limit. From statistical studies of rough surfaces,⁸⁻¹⁰ $N \sim 0.05A_0/Rh_{\text{rms}}$. This gives $NP_c \sim wA_0/4h_{\text{rms}}$, with no explicit dependence on R .

Figure S-3 shows our results for the adhesive force as a function of h_{rms}/δ_c and the prediction of Fuller and Tabor, which is very close to the expressions obtained by Maugis. Note that we plot the maximum force N_{max} obtained as surfaces are brought together, because the pulloff force is

not unique and depends on the peak loading pressure. However the pulloff force is always larger than N_{\max} which would move the numerical data even farther from the theoretical prediction.

It is clear that traditional theories are both quantitatively and qualitatively inconsistent with numerical solutions of the model they were derived for. The predicted pulloff force falls orders of magnitude below the numerical results, and systems with the same value of h_{rms}/δ_c have pulloff forces that vary by almost three orders of magnitude. As noted in the main text, the numerical results depend only on the rms slope and curvature which are predominantly determined by small wavelength roughness. The numerical results do not vary with the long wavelength cutoff of roughness λ_L , while $h_{\text{rms}} \sim \lambda_L^H$ changes more than an order of magnitude.

Fuller and Tabor did not actually use their model to fit their data. They noted that the number of asperities should vary as $1/Rh_{\text{rms}}$ but then dropped this dependence. Instead, they normalized by the pulloff force for smooth surfaces of the same chemistry. The data were then collapsed by fitting δ_c to find an effective radius rather than obtaining R from the actual surface. The resulting radius was about $50\mu\text{m}$, which is much larger than the smallest asperities on typical surfaces. This approach of rescaling both axes to match the theoretical prediction has been typical of subsequent work and masks quantitative errors in the theory. Note that normalizing our numerical data by the smooth surface result, $wA_0/\Delta r$, introduces a parameter that is not present in past theories and does not improve the correlation between pulloff force and h_{rms}/δ_c .

¹ Johnson, K. L. *Contact Mechanics* (Cambridge University Press, 1985).

² Baney, J. M. & Hui, C.-Y. A cohesive zone model for the adhesion of cylinders. *J. Adhesion Sci. Technol.* **11**, 393 (1997).

³ Yang, F. & Cheng, Y.-T. Revisit of the two-dimensional indentation deformation of an elastic half-space. *J. Mater. Res.* **24**, 1976 (2009).

⁴ Derjaguin, B. V., Muller, V. M., & Toporov, Y. P. Effect of contact deformations on the adhesion of particles. *J. Colloid Interf. Sci.* **53**, 314 (1975).

⁵ Maugis, D. Adhesion of spheres: The JKR-DMT transition using a Dugdale model. *J. Colloid Interf. Sci.* **150**, 243 (1992).

⁶ Johnson, K. L., Kendall, K., & Roberts, A. D. Surface energy and the contact of elastic solids. *Proc. R. Soc. Lond. A* **324**, 301 (1971).

- ⁷ Fuller, K. N. G. & Tabor, D. The effect of surface roughness on the adhesion of elastic solids. *Proc. R. Soc. Lond. A* **345**, 327 (1975).
- ⁸ Maugis, D., On the contact and adhesion of rough surfaces. *J. Adhesion Sci. Technol.* **10**, 161 (1996).
- ⁹ Nayak, P. R. Random process model of rough surfaces. *J. Lubr. Technol.* **93**, 398 (1971).
- ¹⁰ Archard, J.-F. Surface topography and tribology. *Tribol. Int.* **7**, 213 (1974).

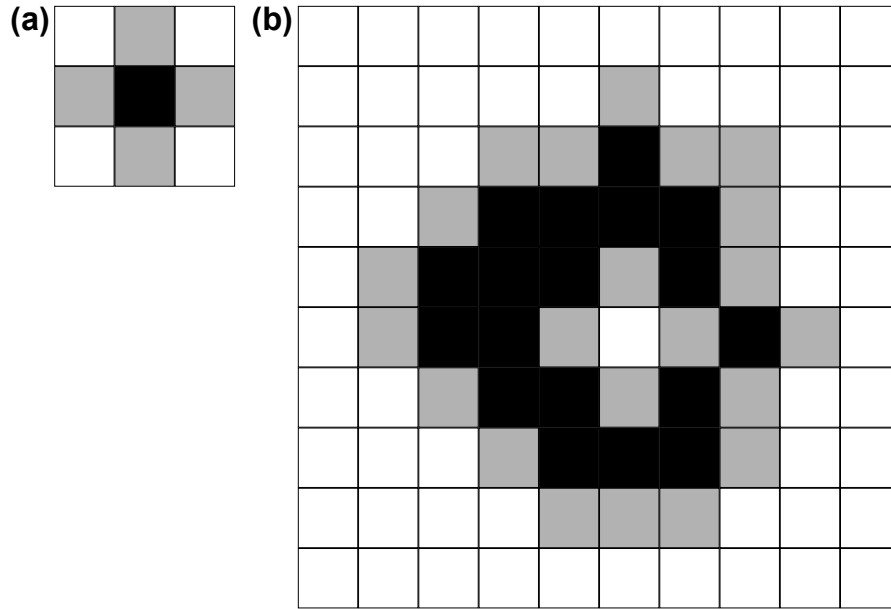


FIG. S-1: **Identifying the contact patch perimeter.** (a) Grid cells are neighbors when they share an edge. Gray squares are neighbors of the black square in the middle. (b) A patch showing perimeter cells with less than four neighbors in gray and interior cells with four neighbors in black.

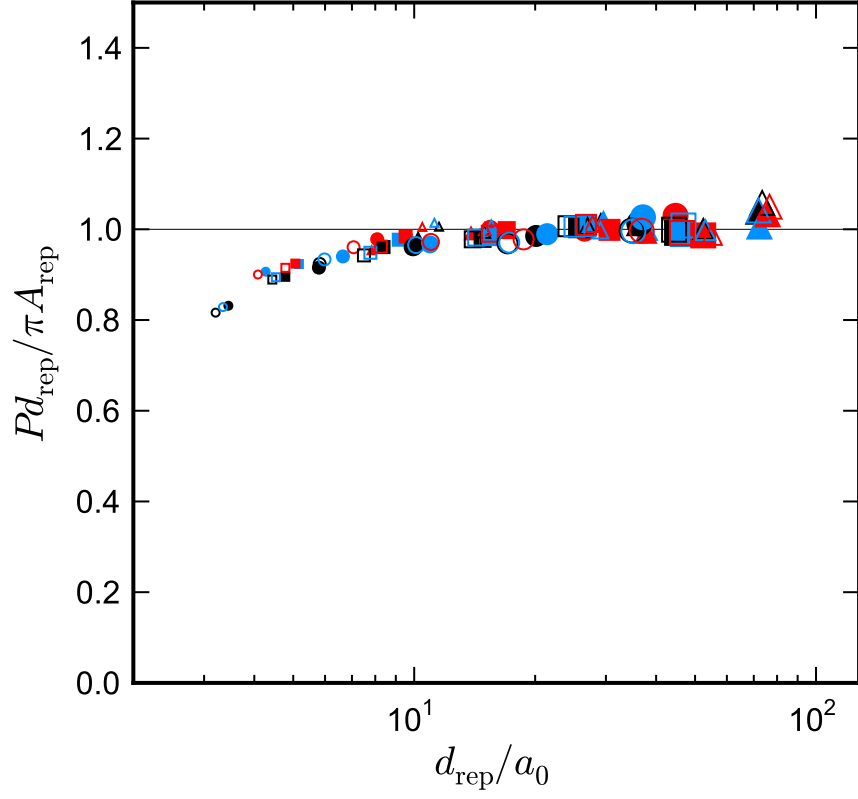


FIG. S-2: **Test of relationship between perimeter P , mean diameter d_{rep} and area A_{rep} .** The ratio of Pd_{rep}/π to repulsive area as a function of the mean width of contacting regions d_{rep} . Results are shown for $H = 0.3$ (triangles), 0.5 (squares) and 0.8 (circles) and $\ell_a/a_0 = 0.0005$ (black), 0.005 (blue) and 0.05 (red). Closed and open symbols are for $h'_{\text{rms}} = 0.1$ and 0.3 , respectively. The symbol size increases as λ_s/a_0 increases from 4 to 64 in powers of 2.

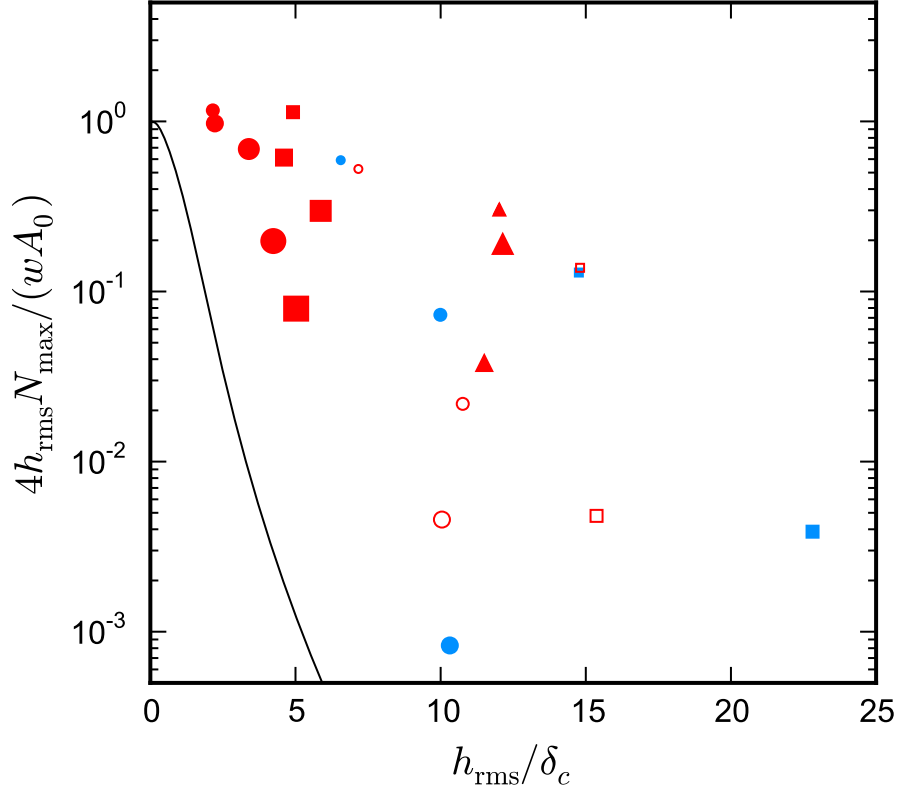


FIG. S-3: **Comparison with Greenwood-Williamson-type theories.** Maximum force N_{\max} upon approach of the two surfaces plotted against the adhesion parameter h_{rms}/δ_c with $\delta_c = 3/4(\pi^2 w^2 R/(E^*)^2)^{1/3}$ identified by Fuller & Tabor.⁷ The force is plotted in units of NP_c where $P_c = 3\pi wR/2$ is the Johnson-Kendall-Roberts⁶ pulloff force for a single sphere and N is the number of asperities. We use the rms curvature to express $1/R = h''_{\text{rms}}/2$ and additionally make use the frequently quoted relationship $Rh_{\text{rms}}N/A_0 = 0.05$.¹⁰ Clearly, there is little correlation between adhesion parameter and maximum force. Results are shown for $H = 0.3$ (triangles), 0.5 (squares) and 0.8 (circles) and $\ell_a/a_0 = 0.005$ (blue) and 0.05 (red). Closed and open symbols are for $h'_{\text{rms}} = 0.1$ and 0.3 , respectively. The symbol size increases as λ_s/a_0 increases from 4 to 64 in powers of 2.